
Ultrastructure and nanomechanical properties of cementum dentin junction

S. P. Ho,¹ M. Balooch,¹ H. E. Goodis,² G. W. Marshall,¹ S. J. Marshall¹

¹Department of Preventive and Restorative Dental Sciences, Division of Biomaterials and Bioengineering, University of California San Francisco, Box 0758, D 2246, San Francisco, California 94143

²Department of Preventive and Restorative Dental Sciences, Division of Endodontics, University of California San Francisco, San Francisco, California 94143

Received 23 May 2003; accepted 31 July 2003

Abstract: The attachment between cementum and dentin has been given several definitions and nomenclature, including: interzonal layer, intermediate cementum, collagen hiatus, Hopewell-Smith's hyaline layer, and more commonly, cementum–dentin junction (CDJ). Understanding the attachment of two structurally dissimilar hard tissues such as cementum and dentin defined by a junction may provide information necessary to engineer functionally graded materials that can be used for efficient tooth restorations in clinical dentistry and other bioengineering applications. Hence, in this study, as a first step toward understanding the CDJ using a biomechanical approach, it was hypothesized that the CDJ between cementum and dentin is a wide zone with mechanical properties significantly lower than the neighboring tissues. The structure of the CDJ was studied using an atomic force microscope (AFM), and site-specific mechanical response of the three regions; cementum, CDJ, and dentin were determined using an AFM-nanoindenter under dry and wet conditions. The AFM results of the CDJ demonstrated a valley under dry conditions and a peak under wet conditions. The magnitude of the depth of the valley was approximately the same as the height of the peak of the CDJ, ranging from 10 to 40 μm . The

nanomechanical properties under dry conditions indicated no significant difference ($p > 0.05$) in elastic modulus and hardness of the CDJ ($E_r = 17.5 \pm 2.7$ GPa, $H = 0.6 \pm 0.1$ GPa) and cementum ($E_r = 18.7 \pm 2.5$ GPa, $H = 0.6 \pm 0.1$ GPa). The mechanical properties of the CDJ were significantly lower ($p \ll 0.05$) than dentin ($E_r = 19.9 \pm 2.9$ GPa, $H = 0.6 \pm 0.1$ GPa) under dry conditions. However, under more relevant hydrated conditions, the mechanical properties of CDJ ($E_r = 3.0 \pm 0.7$ GPa, $H = 0.1 \pm 0.0$ GPa) were significantly lower ($p \ll 0.05$) than those of cementum ($E_r = 6.8 \pm 1.9$ GPa, $H = 0.2 \pm 0.1$ GPa) and dentin ($E_r = 9.4 \pm 2.3$ GPa, $H = 0.3 \pm 0.1$ GPa). Based on the results from this study, it can be concluded that the CDJ can be regarded as a wide zone containing large quantities of proteins including collagen that contribute to hydration and significantly reduce mechanical properties, compared with the adjacent hard tissues, cementum, and dentin. The lower mechanical properties of the CDJ may make it possible for it to redistribute occlusal loads to the alveolar bone. © 2003 Wiley Periodicals, Inc. *J Biomed Mater Res* 68A: 343–351, 2004

Key words: cementum; interface; AFM; nanoindentation; cementum–dentin junction; CDJ

INTRODUCTION

Understanding the attachment of two structurally dissimilar hard tissues such as cementum and dentin could provide information necessary to engineer functionally graded materials that can be used for efficient tooth restorations in clinical dentistry and other bioengineering applications. Cementum is an intermedi-

ate hard tissue that joins root dentin to alveolar bone by way of a periodontal ligament.¹ Cementum, like bone and dentin, is a composite of organic (collagen and other proteinaceous substances) and inorganic (apatite crystals) phases. Generally, cementum is the least mineralized when compared with three other hard tissues: enamel, dentin, and bone. The mineral content on a weight percent basis in cementum is approximately 65% with an organic content of 23% and water the remaining 12%. The bulk of the inorganic phase is composed of apatite, a calcium phosphate mineral, with other trace elements.² The organic phase of cellular cementum is composed of collagen and other extracellular matrix proteins and cells.

The inner part of cementum is attached to root dentin that contains more inorganic apatite phase

Correspondence to: S. J. Marshall; e-mail: sallym@itsa.ucsf.edu

Contract grant sponsor: National Institutes of Health; contract grant number: T32 DE07306

Contract grant sponsor: National Institute of Dental and Craniofacial Research; contract grant number: P01 DE09859

(80%) than cementum.² The bulk of dentin is an acellular biological composite consisting largely of collagen reinforced with apatite and smaller amounts of noncollagenous proteins. Despite the composition similarities, the structures are completely different. The intertubular dentin contains a tubular structure (approximately 1- μm diameter) extending from the surface to the pulp chamber. In transverse sections, the tubules appear to radiate out in all directions from the pulp chamber. Cementum structure is similar to bone, forming a lamellar and trabecular bone-like structure with a lacunae-canalliculi system around the root dentin surface.^{1,2} The mechanical properties of cementum evaluated by Malek et al.³ provided an elastic modulus ranging from 3.99 to 9.9 GPa and hardness from 0.29 to 0.59 GPa. In a review article by Kinney et al.,⁴ the range of elastic modulus assigned to coronal dentin was 18 to 25 GPa whereas the hardness was 0.29 to 0.68 GPa. The structural and chemical composition differences between cementum and dentin result in hard tissues with significantly different mechanical properties.

The region defining the attachment of dentin and cementum has been called the following: the interzonal layer, intermediate cementum, collagen hiatus, Hopewell-Smith's hyaline layer, and most commonly, the cementum-dentin junction (CDJ).⁵⁻⁸ Bodecker⁵ qualitatively examined the region between the two hard tissues and described it as an embryonic remnant of cementum and termed it as an "interzonal layer." Benez⁶ termed the layer an "intermediary layer of cementum," which was later shortened to "intermediate cementum." el Mostehy and Stallard⁷ defined the intermediate zone as a narrow band containing collagen fiber bundles and termed it a "collagen hiatus." Hopewell-Smith⁸ defined the region between cementum and dentin as an amorphous region and named it the "Hopewell-Smith's hyaline layer." However, Yamamoto et al.,⁹ in more recently published work, suggested that the Hopewell-Smith's and intermediate cementum layers are synonymous definitions of the same region between cementum and dentin. Some have suggested that cementum is attached to root dentin by the intermingling of collagen fibrils from both cementum and dentin. However, Yamamoto et al., using enzyme digestion and sodium hydroxide maceration techniques, stated that the CDJ is a narrow zone 1-3 μm wide containing proteoglycans (PGs) with enamel- and bone-related proteins.^{9,10} They concluded that this adhesive layer forms the primary attachment between cementum and dentin, and that the intermingling of the collagen fibrils was less important.^{9,10} In this study, to avoid ambiguity, the natural zone defining the attachment between cementum and dentin is referred to as the CDJ.

Despite the nomenclature and various definitions provided in the literature, limited knowledge exists

about the native structure of the CDJ attaching cementum to dentin. Most current knowledge is based on tissues that were fixed and demineralized or treated with enzymes, which could cause artifacts when evaluating structure and mechanical properties. Thus, the native structure and mechanical properties of the CDJ connecting cementum to root dentin are not completely understood.

It is well documented in engineering that sharp interfaces between materials with a mechanical property mismatch contribute to stress concentrations¹¹ within the interface. This suggests that the narrow interface described by Yamamoto et al.^{9,10} might not be optimized for biomechanical stress distribution and that a wider zone would be more desirable, although the direct region of attachment could correspond to the layers described by Yamamoto et al. Hence, in this study, as a first step toward understanding the CDJ using the biomechanical approach, it was hypothesized that the natural CDJ is a wider zone with lower mechanical properties associated with higher organic content. To evaluate the hypothesis, the objectives of the work were to determine the: (i) native structure of the CDJ, and (ii) nanomechanical properties (elastic modulus and hardness) of the CDJ relative to the adjacent hard tissues, cementum and dentin. The structure of the CDJ was evaluated qualitatively and quantitatively using an atomic force microscope (AFM), and the site-specific mechanical response of the three regions; cementum side of the CDJ (C-CDJ) and dentin side of the CDJ (D-CDJ) and CDJ were determined using an AFM-nanoindenter.

MATERIALS AND METHODS

Thick sections of tooth samples

Mandibular third molars ($n = 5$) of older males with ages ranging from 65 to 80 yr were sterilized using 0.26 Mrad of γ -radiation.¹² Longitudinal and transverse ground sections of 100-200 μm were prepared from half of the tooth. Additionally, transverse sections 5 mm in thickness were obtained from the apical third of the molars using a diamond wafering blade and a low-speed saw (Buehler; Isomet, Lake Bluff, IL) under wet conditions (Fig. 1). The samples were ultrasonicated in deionized water for 10 s (Neysonic Ultrasonicator; UCSF, San Francisco, CA) after preparation to remove any abrasives from coarse sectioning using the diamond blade. The 5-mm-thick transverse sections were glued to AFM steel stubs (Ted Pella, Inc., Redding, CA) using a cyanoacrylate adhesive (MDS Products Inc., CA) for ultra-sectioning using an ultramicrotome and a diamond knife.

Ground sections 100-200 μm thick were prepared using basic metallography polishing techniques. The longitudinal and transverse ground sections ($n = 5$ each) were prepared by initially polishing using a series of silicon carbide grit

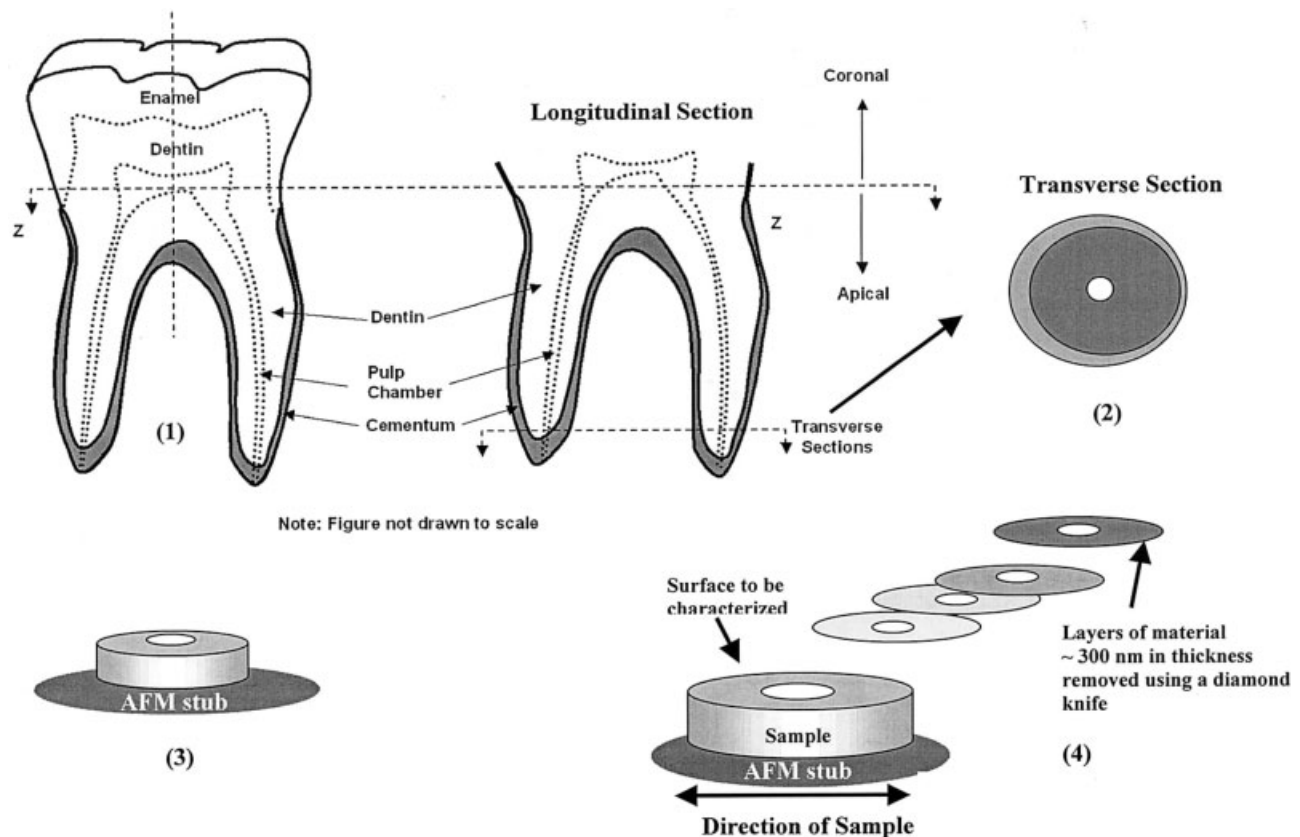


Figure 1. Schematic of a molar and longitudinal section (1), transverse sections (2), sample mounted on an AFM steel stub (3), and ultrasectioned sample surface (4).

paper with sizes 240, 400, 600, 800, 1200, and 2400 (Buehler). The fine polishing of both surfaces was performed using a diamond suspension slurry of grades 6, 3, 1, 0.5, 0.25, and 0.1 μm (Buehler). The samples were ultrasonicated for 10 s each before proceeding to the next finer level of polishing. The CDJ within the ground sections was studied under wet conditions using deionized water. Qualitative analysis of the CDJ was performed using transmission light microscopy with an Image-Pro software (Image-Pro Plus Microscope, version 4.0; Media Cybernetics, Silver Spring, MD). A series of micrographs was taken and carefully placed in sequential order to examine the structure of dentin, CDJ, and cementum.

Ultrasectioning of tooth samples

The mounted transverse samples were placed in an ultramicrotome (Ultracut E, Reichert-Jung, Reichert Scientific Instrument Technical Services, GA) ensuring that the final sectioned surface would retain a high degree of flatness (Fig. 1). The samples were sectioned using a glass knife (Electron Microscopy Laboratory, UCSF) set at a cutting angle of 6° and a cutting speed of 0.75 mm/s. The final trimming of the sample was performed using a diamond knife (Micro Star Technologies, Huntsville, TX) at an angle of 4.5° and a cutting speed of 0.75 mm/s. The 300-nm-thick ultrasections were removed from the sample and discarded (Fig. 1). The

microtomed surface of the remaining specimen block was characterized using an AFM and an AFM-nanoindenter. The microtome surface preparation method was selected based on preliminary experiments that demonstrated that a flat surface with structural features similar to cryofractured scanning electron microscopy surfaces was produced by the method, as shown in Figure 1. Polishing introduced artifacts and these structures were obscured.

Atomic force microscopy of the ultrasectioned sample surfaces

The topographies of the ultrasectioned surfaces under dry and wet conditions were scanned using a contact mode AFM (Nanoscope III, Multimode; DI-Veeco Instruments Inc., Santa Barbara, CA). The surface probing was performed using a Si_3N_4 tip attached to a “V-shaped” type “D” microlever with a nominal normal spring constant of 0.03 N/m (Thermo Microscopes, CA) at a scanning frequency of 0.5 Hz. The nominal radius of curvature of the tip was <50 nm. To obtain statistically significant data for the size of the CDJ, three different areas ($n = 3$) on each ultrasectioned sample ($n = 5$) were scanned. Areas as large as $100 \times 100 \mu\text{m}^2$ were evaluated using a “J” type piezo scanner. For higher resolution examination, smaller areas of $25 \times 25 \mu\text{m}^2$ were also examined and the size of the CDJs was determined using the scanned areas and Nanoscope III version 4.43r8

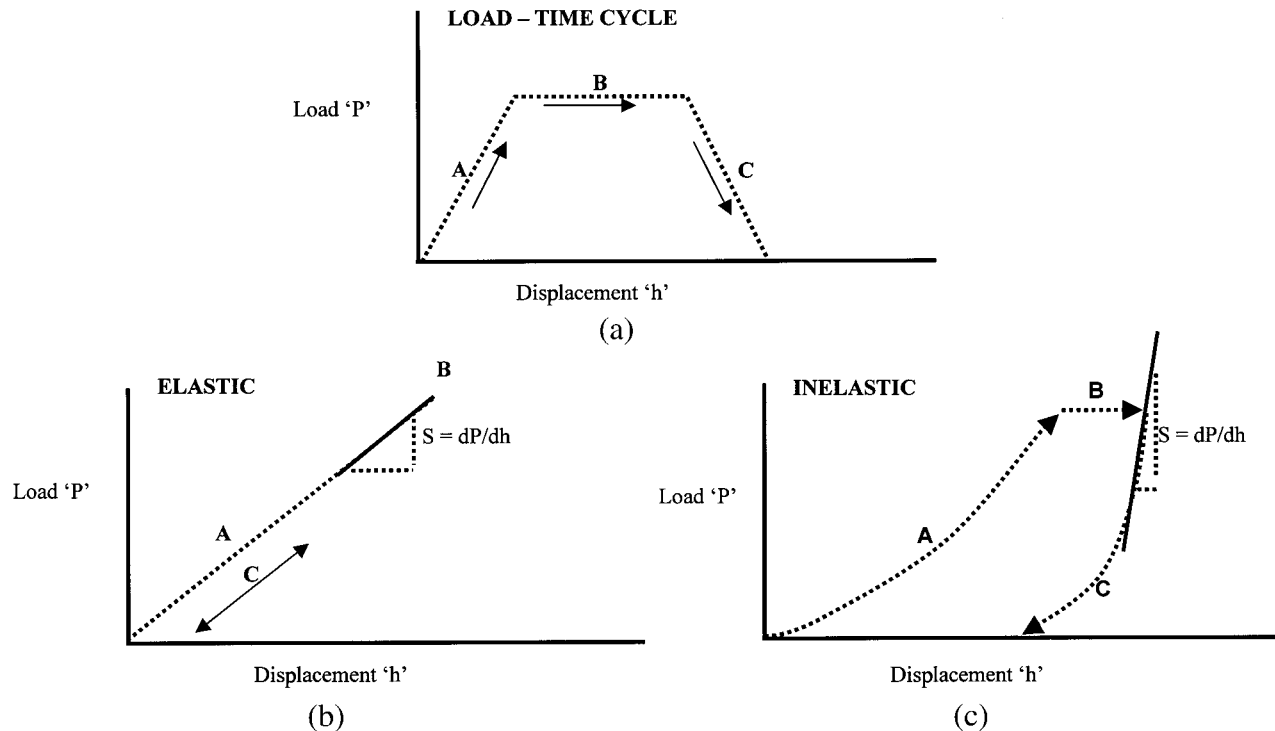


Figure 2. (a) Representative load-time curve for a material with phase A = loading, phase B = holding, and phase C = unloading. In this study, each phase was 3 s with a total loading–unloading cycle of 9 s. (b) Representative load-displacement response for an elastic material where A = loading, B = hold (represented by a point in this case), and C = unloading (retracing the loading path). (c) Representative load-displacement response for an inelastic material where A = loading, B = hold, and C = unloading. Phase B of this curve illustrates the influence of time-dependent properties and in phase C the first 25% of the curve represents elastic recovery. The slope “S” is used to calculate the elastic modulus of a material using Equation (1) shown within the text. Phases A and C do not overlap, illustrating permanent deformation within the material.

software (Nanoscope III, Multimode; DI-Veeco Instruments, Inc.).

Nanoindentation of the ultrasectioned samples

Nanomechanical tests on dry and wet samples ($n = 5$ each) were performed using an AFM, to which a load-displacement transducer (Triboscope Micromechanical Test Instrument Hysitron Inc., Minneapolis, MN) was attached. A sharp diamond Berkovich indenter with a radius of curvature <100 nm (Triboscope Micromechanical Test Instrument; Hysitron Inc.) was fitted to the transducer. The scan speed, scan area, and load displacement of the indenter on the sample material were controlled by a computer.¹³ The AFM piezo and respective control systems were used to image the surface of the sample to find a specific site of interest after which the load-displacement transducer was used to indent the sample while collecting the load displacement data. After indentation, the AFM piezo was used to scan the indented area. However, if the indented areas are small and the sample surface is textured, it is difficult to distinguish the indents. Nanoindentation under wet conditions was performed by immersing the sample and the indenting probe in deionized water. The indents were made on sample areas of $50 \times 50 \mu\text{m}^2$ with a minimum of 20 indents on each area. The maximum load used was $1000 \mu\text{N}$

[Fig. 2(a)]. Fused silica was used as a calibration standard for the AFM-nanoindenter despite its limitations, especially for softer materials, as stated by other researchers.¹⁴

In a typical indentation experiment, the load time curve involves engaging the indenter with the sample surface and loading to a specified maximum, causing indentation into the surface and subsurface layers, holding at the maximum load for a few seconds, and then unloading at the same rate as for the loading [Fig. 2(a)]. A load-displacement curve for purely elastic materials involves no displacement during the hold phase and a full recovery of the material with the unload phase retracing its path over the load phase [Fig. 2(b)]. However, in the case of materials such as polymers and tissues that exhibit time-dependent properties, namely, viscoelasticity, a significant displacement occurs during the hold phase, with a partial recovery of the material, and the unload phase does not retrace its path over the load phase [Fig. 2(c)]. The unloading data are used to determine the mechanical properties based on classical indentation theory introduced by Boussinesq,¹⁵ simplified by Sneddon,¹⁶ and generalized by Pharr et al.¹⁷ According to this theory, a material experiences elastic recovery during the first 25% of the unloading phase of the load–unload curve. The slope (dP/dh) where P is the load and h is the indentation displacement, is used to determine the stiffness S of the material, from which the reduced elastic modulus is determined using Equations (1) and (2) as follows:

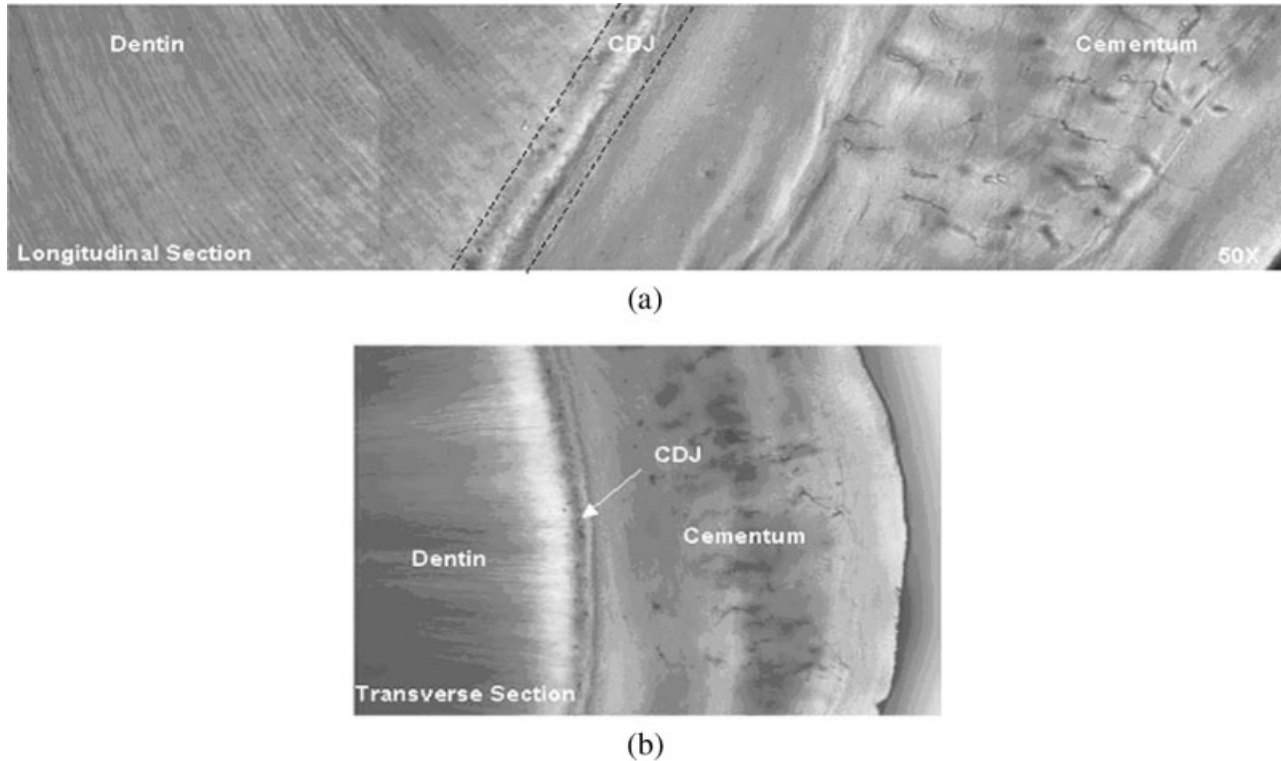


Figure 3. Light microscopy micrographs of (a) longitudinal and (b) transverse ground sections illustrating the CDJ between the two hard tissues, cementum, and dentin. The micrographs were taken under wet conditions using a transmission light microscope and Image-Pro Plus software.

$$S = \frac{2E^*A_{\max}^{1/2}}{\pi^{1/2}} \quad (1)$$

where A_{\max} is the projected surface contact area at the maximum displacement, and E^* is the reduced elastic modulus given by:

$$E^* = \left[\frac{1 - \nu_s^2}{E_s} + \frac{1 - \nu_i^2}{E_i} \right]^{-1} \quad (2)$$

where E and ν are the elastic modulus and Poisson’s ratio and subscripts i and s denote the indenter and specimen materials, respectively. However, the moduli of polymers are significantly lower than the elastic modulus of a diamond, which reduces Equation (2) to $E^* = [(1 - \nu_s^2)/E_s]^{-1}$. After mathematical simplification, the reduced elastic modulus and hardness of a sample can be determined using the following equations:

$$E^* = \left[\frac{1}{2} \left(\frac{\pi}{A_{\max}} \right)^{1/2} S \right] \quad (3)$$

$$H = \left[\frac{P_{\max}}{A_{\max}} \right] \quad (4)$$

where A_{\max} is the maximum projected area for the maximum specified load P_{\max} . For the current state of art nanoindentation equipment, the models used to determine the nanomechanical properties do not account for the time-dependent behavior of polymeric materials, both natural and synthetic, in addition to the pile-up effects as stated by Van Landingham et al.¹⁸ in a comprehensive overview

about nanoindentation of polymers. Hence, it is important to note that the nanomechanical properties evaluated in this study were used to determine the relative differences between the CDJ, cementum, and dentin. This approach has been used extensively to study dentin and enamel, but not for cementum or CDJ.^{19,20}

RESULTS

Light microscopy of ground sections

The ground sections consistently illustrated a wide CDJ between cementum and dentin in all samples [Fig. 3(a)]. Moreover, the CDJ also was found within the transverse sections as shown in Figure 3(b). However, at this resolution, it was difficult to study the structure or mechanical properties of the zone relative to its adjacent tissues. The cementum hard tissue was identified by the lacunae-canalliculi structure and dentin was identified by its tubular structure (Fig. 3).

Atomic force microscopy of CDJ

The width of the CDJ determined using an AFM indicated a range of 13–40 μm . AFM scans represen-

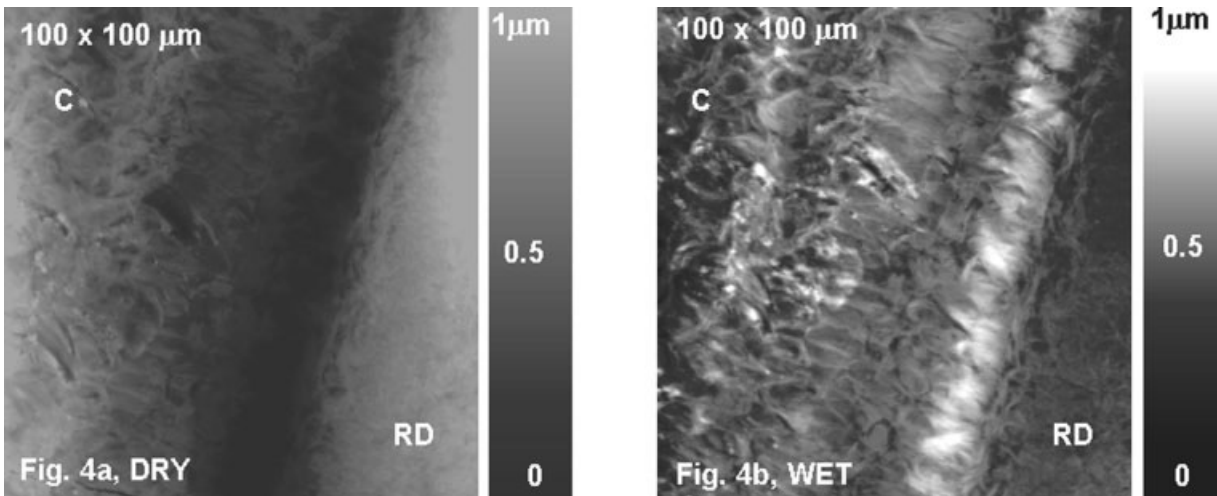


Figure 4. AFM micrographs $100 \times 100 \mu\text{m}^2$ of the ultrasectioned samples illustrating the CDJ under (a) dry and (b) wet conditions. Note: the CDJ absorbs water significantly relative to the adjacent hard tissues, cementum "C" and root dentin "RD" under hydrated conditions.

tative of the CDJ at a lower resolution with a scan area of $100 \times 100 \mu\text{m}^2$ and a higher resolution of $25 \times 25 \mu\text{m}^2$ under dry and wet conditions are shown in Figures 4 and 5. In all cases, the CDJ resembled a valley under dry conditions [Fig. 4(a)]. However, under wet conditions, the CDJ appeared to be a peak, indicating an increase in height [Fig. 4(b)]. Section plots of the

AFM micrographs (Fig. 5) indicated that the magnitude of the depth of the valley under dry conditions [Fig. 5(a)] was approximately equal to the height of the peak under hydrated conditions [Fig. 5(b)]. The trend between the dry and wet conditions at both high and low resolutions was the same. The hydration of the CDJ was consistently higher compared with the im-

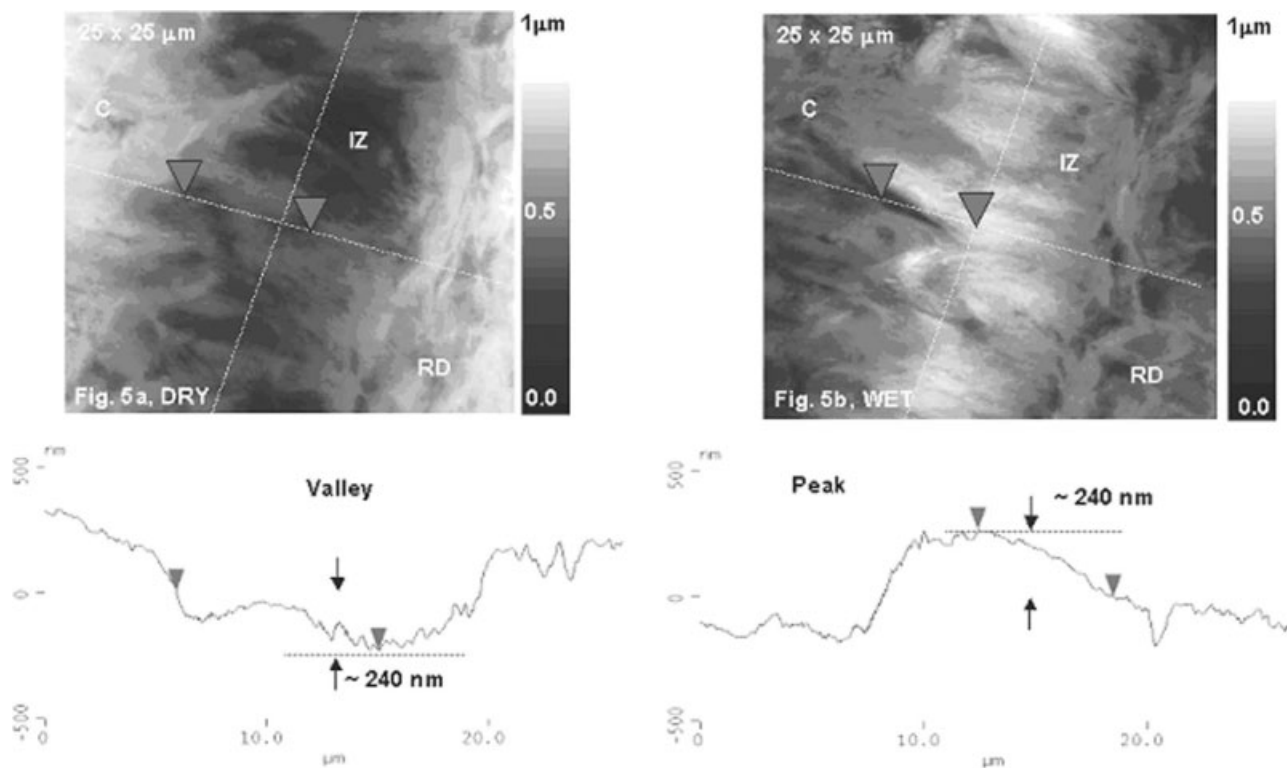


Figure 5. Section plots of the AFM micrographs of $25 \times 25 \mu\text{m}^2$ areas. (a) Under dry conditions, the CDJ is a valley between cementum "C" and root dentin "RD." (b) Under hydrated conditions, the same CDJ between the two hard tissues absorbs water and is a peak. In this analysis, the magnitude of the depth of the valley under dry conditions was approximately the same as the height of the peak under wet conditions.

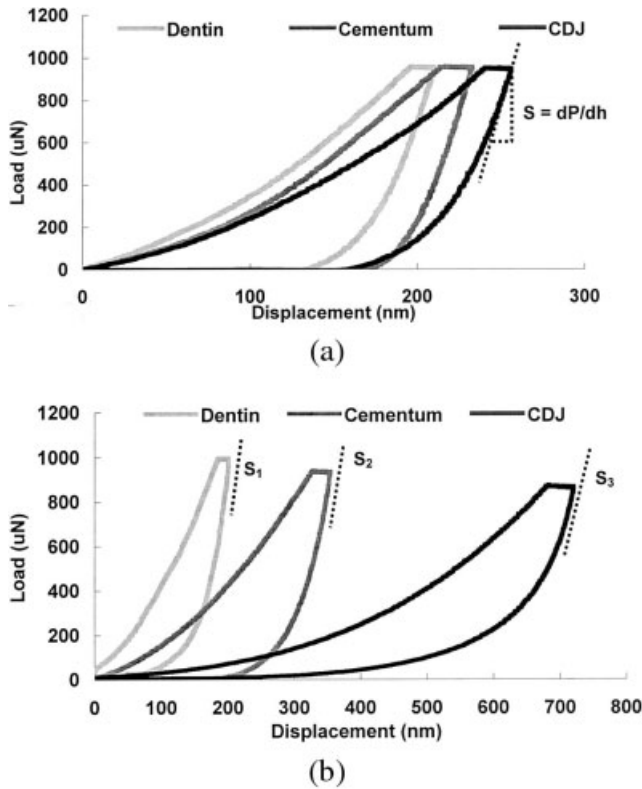


Figure 6. Representative load-displacement curves for the three regions, cementum, dentin, and CDJ under (a) dry and (b) wet conditions. (a) Notice that the slope that defines the stiffness “S” during the first 25% of the unloading curve is similar for all three regions under dry conditions. (b) Notice that the slopes “S₁,” “S₂,” and “S₃” are different for all three regions under wet conditions.

mediate adjacent hard tissues for all samples (*n* = 5) (Figs. 4 and 5).

Nanomechanical properties of cementum, dentin, and CDJ

The nanomechanical response of the three regions (C-CDJ, CDJ, D-CDJ) under dry conditions indicated that the stiffness of D-CDJ, C-CDJ, and CDJ was similar (Fig. 2). Additionally, each region exhibited similar displacement during the hold phase “B” for 3 s at 1000 μN of the loading–unloading experimental cycle [Fig. 6(a)].

The nanomechanical response of the three regions varied when hydrated as shown by the stiffnesses “S₁,” “S₂,” and “S₃” [Fig. 6(b)]. Additionally, the hold phase of the loading–unloading experimental cycle exhibited higher displacement for the CDJ compared with the cementum side and the dentin side of the CDJ [Fig. 6(b)]. The displacements during the hold phase were higher for all three regions under wet conditions [Fig. 6(b)] compared with dry conditions [Fig. 6(a)].

TABLE I
Reduced Elastic Modulus and Hardness Values for Cementum, Dentin, and CDJ Under Dry Conditions

Characterized Regions (Dry)	Reduced Elastic Modulus <i>E_r</i> ± SD (GPa)	Hardness <i>H</i> ± SD (GPa)
Cementum	18.67 ± 2.50 <i>p</i> = 0.05*	0.59 ± 0.13 <i>p</i> = 0.12*
Dentin	19.89 ± 2.69 <i>p</i> ≤ 0.05*	0.65 ± 0.12 <i>p</i> ≤ 0.05*
CDJ	17.48 ± 2.69	0.56 ± 0.12

**p* values are relative to the CDJ, with a confidence level of 95%.

A Student’s *t* test with 95% confidence level indicated no significant difference (*p* = 0.05) in elastic modulus and hardness between CDJ and C-CDJ under dry conditions. However, the elastic modulus and hardness of CDJ were significantly lower (*p* ≤ 0.05) than D-CDJ under dry conditions [Table I, Figs. 7(a)]. Under wet conditions, the elastic modulus and hardness of CDJ were significantly lower (*p* ≤ 0.05) than C-CDJ and D-CDJ [Table II, Figs. 7(b)]. The mechanical properties of C-CDJ, CDJ, and D-CDJ under dry conditions were approximately 50, 63, and 80% higher than the respective regions under wet conditions. The *p* values shown in Tables I and II are relative to the CDJ, with a confidence level of 95%.

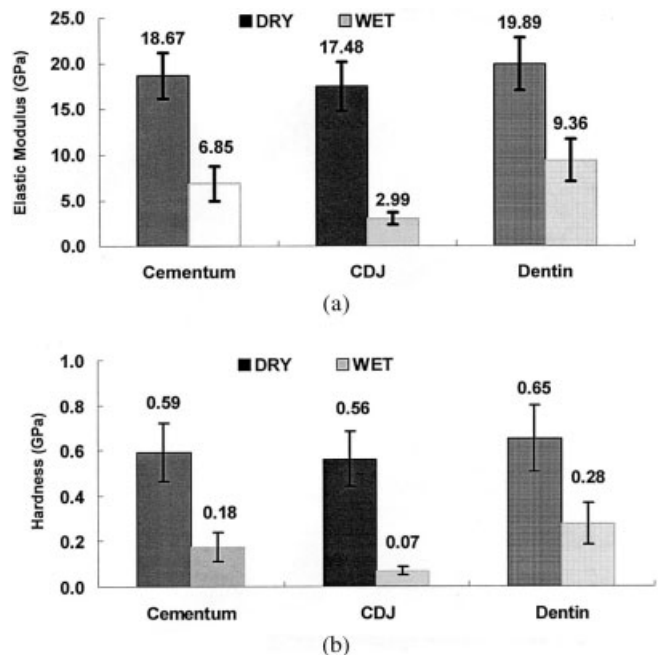


Figure 7. Reduced elastic moduli and hardness values for the three regions under (a) dry and (b) wet conditions for cementum, dentin, and CDJ. Note: the values for cementum and dentin are representative of the areas very adjacent to the CDJ.

TABLE II
Reduced Elastic Modulus and Hardness Values for
Cementum, Dentin, and CDJ Under Wet Conditions

Characterized Regions (Wet)	Reduced Elastic Modulus $E_r \pm SD$ (GPa)	Hardness $H \pm SD$ (GPa)
Cementum	6.85 ± 1.91 $p \ll 0.05^*$	0.18 ± 0.06 $p \ll 0.05^*$
Dentin	9.36 ± 2.32 $p \ll 0.05^*$	0.28 ± 0.09 $p \ll 0.05^*$
CDJ	2.99 ± 0.65	0.07 ± 0.02

* p values are relative to the CDJ, with a confidence level of 95%.

DISCUSSION

The results of this study confirm the hypothesis that the natural CDJ between cementum and dentin is a wide zone with mechanical properties relatively lower than the immediately adjacent hard tissues (C-CDJ and D-CDJ). Scanning the surfaces of the ultrasectioned samples using an AFM facilitated the analysis of the structural characteristics of the CDJ in both dry and wet conditions. Testing in a wet environment simulated *in vivo* conditions. The consistent expansion of the CDJ under wet conditions [Figs. 4(b) and 5(b)] suggests that it contains hydrophilic and lower mineral content constituents, such as collagenous and noncollagenous proteins. This region of altered composition could facilitate both biological and biomechanical functions in addition to providing structural integrity of the CDJ.

The CDJ is thought to have a high PG content, as well as collagen content.⁹ PGs could contribute to the structural integrity of the CDJ, especially under wet conditions. The PGs act as hydrophilic monomers in association with other more or less hydrophilic polymers such as collagen, in both hard and soft tissues. To date, works by Bartold et al,^{21,22} Cheng et al.,²³ and Yamamoto et al.,²⁴ confirmed the existence of PGs within bulk cementum as well as within the zone that connects cementum to root dentin. Cementum contains various glycosaminoglycans including chondroitin sulfate and probably small amounts of hyaluronan and dermatan sulfate.²¹ Yamamoto et al.,²⁴ using enzymes such as hyaluronidase and trypsin, concluded that PGs were localized within a narrow zone of 1–3 μm in thickness, which they termed the CDJ. Bartold et al.²² have shown that these molecules have a larger distribution by demonstrating chondroitin sulfate PGs in the pericellular spaces within the lacunae and in the extracellular spaces of cementum. Localization of lumican and fibromodulin PGs in precementum walls of the lacunae and cementocytes have recently been shown in bovine bulk cementum by Cheng et al.²³ The existence of various PGs

within cementum is convincing, but the existence of PGs within a limited width of 1–3 μm between cementum and dentin needs more investigation. From this work, it appears that a 10–40- μm region exists that is sensitive to hydration, contains low mineral content, and may represent a broad region of PG-rich tissue.

The significantly higher hydration effects observed in this study over a CDJ width of 10–40 μm (Figs. 4 and 5) could be attributed to the ability of the PGs to retain large quantities of water, occupying space, thus cushioning or lubricating other structures.²⁵ The large number of —OH groups and negative charges on the molecules, which could separate carbohydrate chains, may aid in the observed hydration effects within the CDJ (Figs. 4 and 5).²⁵ The high density of negative charges attracts water, forming a hydrated gel (hydrogel) similar to cartilage. In this study, the hydration effects in the 10–40- μm zone may indicate that the localization of PGs is not limited to a narrow zone of width 1–3 μm . However, a real time study using an AFM and involving selective removal of PGs by enzyme digestion could confirm the spatial distribution of the PGs within the CDJ and its adjacent hard tissues.

The significantly lower nanomechanical properties of the CDJ and higher displacements for the same normal load of 1000 μN under wet conditions [Figs. 6(b) and 7(b), Tables I and II] suggest a lower mineral content compared with cementum and dentin. Under wet conditions, the mechanical resistance to loading for the CDJ could be attributed to the presence of hydrated PGs and collagen fibrils, and a lower amount of apatite crystals. The mechanical response of the adjacent regions demonstrates a higher amount of apatite crystals, the content being higher for dentin than cementum.²

Viscoelastic properties become important because of the presence of organic constituents of noncollagenous and collagenous proteins in significant amounts within these regions. These characteristics become evident during the “hold” portion of the loading cycle. As might be expected, they were most apparent under wet conditions [Fig. 6(b)]. Although the evaluation of mechanical properties allowed us to demonstrate this characteristic, it is not an optimized technique for determining viscoelastic properties and additional work is needed.

Depending on the testing environment conditions (dry or wet), the mechanical response of a constituent in a composite material may become dominant, subsequently causing a change in the total mechanical response of the tissue. In this study, all three materials exhibited some viscoelasticity under dry and wet conditions (Fig. 6). However, the dominance of viscoelasticity was higher for the CDJ compared with cementum and dentin under wet conditions [Fig. 6(b)], because the CDJ is a softer material composed of

predominantly hydrophilic organic nanoconstituents when compared with cementum and dentin [Figs. 6(b) and 7, and Table II]. Although cementum and dentin are more fortified with mineral, they continue to exhibit some viscoelasticity. Under dry conditions, the underlying harder matrix dominates, forming a valley and contributing to higher mechanical and similar time-dependent properties as the immediately adjacent hard tissues (C-CDJ and D-CDJ) [Figs. 5(a) and 6(a), and Table I]. The less mineralized organic constituents may shrink, leading to the apparent overestimation of the hardness and elastic modulus. Similar effects recently have been reported for partially demineralized caries dentin.²⁶

CONCLUSIONS

The results of this study show that the CDJ between human cementum and dentin is a wide zone of lower mechanical properties, probably because of lower mineral content and higher organic content. The lower mechanical properties of the CDJ in addition to a larger width could facilitate in reducing the stress concentrations between mechanically dissimilar tissues such as cementum and dentin. The softer and wider CDJ would aid in cushioning and lubricating as well as allowing the passage of nutrients between cementum and dentin. The overall function of the CDJ could aid absorption and distribution of occlusal loads between cementum and dentin before release into the alveolar bone. Future studies should be performed to determine the strain distributions across the CDJ in relation to cementum and dentin as well as the alveolar bone. Finite element methods and Moiré interferometry techniques at micrometer and larger scales may lead to a better understanding of such mechanisms.

This work was supported by the National Institutes of Health (S. P. Ho) and the National Institute of Dental and Craniofacial Research. The authors thank Dr. John Greenspan for the use of the ultramicrotome and Vibecka Peterson for her expertise in the use of the instrument. Additionally, the authors thank Grace Nonomura for supplying the samples used in this study.

References

1. Ten Cate AR. Oral histology, development, structure and function. 5th ed. St. Louis, MO: Mosby-Year Book, Inc.; 1998.
2. Mjor IA, Fejerskov O. Histology of the human tooth. 2nd ed. Munksgaard: Scandinavian University Books; 1979. p 105–114.
3. Malek S, Darendeliler MA, Swain MV. Physical properties of root cementum. I. A new method for 3-dimensional evaluation. *Am J Orthod Dentofacial Orthop* 2001;120(2):198–208.
4. Kinney JH, Marshall SJ, Marshall GW. The mechanical properties of human dentin: a critical review and re-evaluation of the dental literature. *Crit Rev Oral Biol Med* 2003;14(1):13–29.
5. Bodecker CFW. The distribution of living matter in human dentine, cement, and enamel. *Dental Cosmos* 1957;20:582–590.
6. Benz L. Befunde an der Dentinzement Grenze. *Z Stomat* 1927;5:877–896.
7. el Mostehy MR, Stallard RE. Intermediate cementum. *J Periodontal Res* 1968;3:24–29.
8. Hopewell-Smith A. Concerning human cementum. *J Dent Res* 1920;2:59–76.
9. Yamamoto T, Domon T, Takahashi S, Islam N, Suzuki R, Wakita M. The structure and function of the cemento-dentinal junction in human teeth. *J Periodontal Res* 1999;34:261–268.
10. Yamamoto T, Domon T, Takahashi S, Islam MN, Suzuki R. The fibrous structure of the cemento-dentinal junction in human molars shown by scanning electron microscopy combined with NaOH-maceration. *J Periodontal Res* 2000;35:59–64.
11. Borese AP, Schmidt RJ, Sidebottom OM. *Advanced mechanics of materials*. New York: John Wiley & Sons, Inc.; 1993. p 560–561.
12. White JM, Goodis HE, Marshall SJ, Marshall GW. Sterilization of teeth by gamma-radiation. *J Dent Res* 1994;73(9):1560–1567.
13. Triboscope nanomechanical test system setup and operation guide. *Nanomechanical Test Instruments*. Minneapolis, MN: Hysitron Inc.; 1996.
14. Klapperich C, Komvopoulos K, Pruitt L. Nanomechanical properties of polymers determined from nanoindentation experiments. *J Tribol T-ASME* 2001;123:624–631.
15. Strojny A, Xia X, Tsou A, Gerberich WW. Techniques and consideration for nanoindentation measurements of polymer thin film constitutive properties. *J Adhes Sci Technol* 1998;12:1299–1321.
16. Sneddon IN. The relation between load and penetration in axisymmetric Boussinesq problem for a punch of arbitrary profile. *Int J Eng Sci* 1965;3:47–57.
17. Pharr GM, Oliver WC, Brotzen FR. On the generality of the relationship among contact stiffness, contact area, and elastic modulus during indentation. *J Mater Res* 1992;7:613–617.
18. Van Landingham MR, Villarrubia JS, Guthrie WF, Meyers GF. Nanoindentation of polymers: An overview. In: Tsukruk VV, Spencer ND, editors. *Macromolecular symposia 167: Advances in scanning probe microscopy of polymers*. New York: John Wiley & Sons; 2001. p 15–44.
19. Habelitz S, Marshall SJ, Marshall GW, Balooch M. Mechanical properties of human dental enamel on the nanometer scale. *Arch Oral Biol* 2001;46(2):173–183.
20. Marshall GW, Balooch M, Gallagher RR, Gansky SA, Marshall SJ. Mechanical properties of the dentinoenamel junction: AFM studies of nanohardness, elastic modulus, and fracture. *J Biomed Mater Res* 2001;54(1):87–95.
21. Bartold PM, Miki Y, McAllister B, Narayanan AS, Page RC. Glycosaminoglycans of human cementum. *J Periodontal Res* 1988;23:13–17.
22. Bartold PM, Reinboth B, Nakae H, Narayanan AS, Page RC. Proteoglycans of bovine cementum: isolation and characterization. *Matrix* 1990;10:20–29.
23. Cheng H, Catterson B, Yamauchi M. Identification of immunolocalization of chondroitin sulfate proteoglycans in tooth cementum. *Connect Tissue Res* 2002;40(1):37–47.
24. Yamamoto T, Domon T, Takahashi S, Islam N, Suzuki R, Wakita M. The structure and function of the cemento-dentinal junction in human teeth. *J Periodontal Res* 1999;34:261–268.
25. Murray RK, Granner DK, Mayes PA, Rodwell VW. *Harper's biochemistry*. 23rd ed. Norwalk, CT: Appleton & Lange; 1993.
26. Zheng L, Hilton JF, Habelitz S, Marshall SJ, Marshall GW. Dentin caries activity status related to hardness and elasticity. *Eur J Oral Sci* 2003;111:243–252.